9th ECCOMAS Thematic Conference on the Mechanical Response of Composites
COMPOSITES 2023
G. Catalanotti, H. Petterman and G. Pittaresi (Eds)

NUMERICAL SIMULATION OF THE FATIGUE DAMAGE GROWTH IN UNIDIRECTIONAL COMPOSITES BASED ON FIBRE-MATRIX DEBONDING

Alexander Seidel[1*], Bent F. Sørensen[2] and Klaus Drechsler[1]

[1] Chair of Carbon Composites, TUM School of Engineering and Design,
Technical University of Munich, Boltzmannstr. 15, 85748 Garching, Germany
[2] Composites Analysis and Mechanics, Department of Wind and Energy Systems,
Technical University of Denmark, Risø Campus, Frederiksborgvej 399, 4000 Roskilde, Denmark
* alexander.seidel@tum.de

Keywords: Numerical Modelling, Fatigue, Micromechanics

Summary: *A methodology for investigating the micromechanical fatigue behaviour of unidirectional composites based on fibre-matrix debonding is developed. The fatigue damage mechanism is based on the progressive failure of fibres caused by debond crack tip stress fields resulting from fibre breaks in previous load cycles. The methodology combines an analytical model to describe the debond crack initiation and growth with a numerical finite element model to calculate resulting stresses. The methodology is applied on a two-fibre model composite. It can qualitatively predict the stress development within the simulation domain as well as the mechanism of a debond crack tip stress field triggering a break in a neighbouring fibre. Both is consistent with microscale observations in the literature.*

1 Introduction

Modern-day wind turbines are equipped with increasingly longer rotor blades. As these blades consist dominantly of composite materials, understanding their mechanical behaviour, especially the fatigue mechanisms, will be crucial for an optimised blade design.

The fatigue properties of unidirectional fibre-reinforced plastics (UD-FRPs) are usually determined utilising empirical design approaches requiring time-consuming experiments on the coupon level [1]. Additionally, these methods underestimate the actual fatigue performance of the material itself since side effects (like failure initiating in the tab region) lead to a premature failure causing a lower number of cycles to failure than the true fatigue life [2]. A model describing the basic microscopic mechanisms of fatigue in UD-FRPs can help in better understanding the development of fatigue damage zones in this material class and eventually lead to new composite materials with superior fatigue properties. Thus, in the scope of this work, a combined analytical-numerical approach will be proposed to effectively predict the microscale fatigue evolution. The model will be applied on a common material combination of E-glass fibres and epoxy resin used in wind applications. The numerical finite element (FE) simulations are carried out using *Abaqus FEA* by *Dassault Systèmes Simulia Corp.* [3].

2 Methodology for Predicting the Fatigue Damage Evolution

2.1 Overview of the Methodology

The methodology presented in this work builds upon an analytical model introduced by Sørensen [4] and further developed by Sørensen and Goutianos [5] and Sørensen et al. [6]. Conceptually, the model is built upon the microscale fatigue damage evolution documented by Jespersen and Mikkelsen [7]. The analytical model can be used to predict the growth rate of damage zones in UD-FRPs caused by cyclic loading. The main underlying mechanism is that, during first loading, a break in a single fibre leads to a debonding of the fibre and the matrix in a region of certain length around the fibre break. This debonding forms two circular debond crack tips (one in either direction of the fibre break) creating a stress concentration field (in linear elastic fracture mechanics modelled as a singular stress field, denoted the K-field). The primary stress field from the fibre break as well as the secondary stress fields form the debond crack tips result in three distinct stress peaks in a neighbouring fibre of a broken fibre as shown by van den Heufel, Peijs and Young [8]. The debond crack growth during cyclic loading is driven by the mutual influence of forward and backward slip in the debonded interface region and the resulting change in the stress intensity factor ΔK. The details of this mechanism shall not be explained in detail herein. Therefore, the reader is referred to [5]. As the debond crack tip progresses, so does the K-field. The K-field can ultimately reach a microscopic defect in a neighbouring fibre and thus trigger a secondary fibre break. This procedure repeats for further cyclic loading. The debond crack tip of the broken fibre is assumed to eventually reach a constant length where there is no more debond crack growth ($\Delta K = 0$). If all broken fibres in the composite reach that saturated state, a fatigue limit of the composite exists where the growth of the fatigue damage zone comes to a rest. Conversely, if at least always one broken fibre triggers a break in a neighbouring fibre, the fatigue damage zone will grow until the remaining fibres cannot withstand the macroscopic force any more and ultimate failure occurs.

The workflow of the proposed methodology is depicted in Figure 2. For simplicity, the workflow will be explained in the following sections using a two-fibre composite as shown in Figure 1. The two-fibre composite consists of two equivalent fibres of radius r. The distance between the surfaces of these two fibres is denoted as inter-fibre distance d_{if}. The model domain is assumed to be long compared to the fibre radius ($l_{model} \gg r$). The two fibres are surrounded by a thin fibre-matrix interphase layer of finite thickness t_{int}. A fibre coordinate system will be used coherently throughout this work with the fibres being oriented along the z-direction and the fibres being stacked along the y-direction.

Starting from the mathematical formulation of the previous works, the following sections will explain the undertaken steps to adapt the analytical model eventually leading to the newly proposed hybrid analytical-numerical model. The steps from Figure 2 will be given in brackets in the section headings for better understanding.

2.2 Analytical Model for Debond Initiation and Growth (5, 7b, 10)

First Loading and Debond Initiation The two-fibre composite is loaded for the first time up to the maximum applied macroscopic strain $\bar{\varepsilon}_{max}$. During this step, Fibre 1 fails (due to a microscopic defect). Fibre 2 is assumed to not fail in the near proximity of

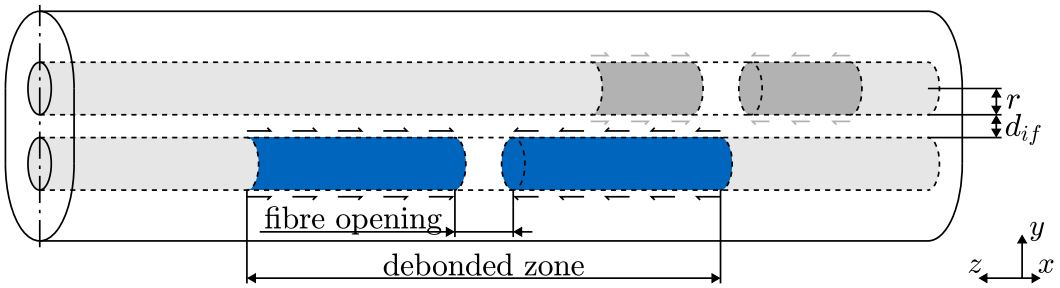

Figure 1: Two-fibre composite after many cycles. FIBRE 1 (blue) is assumed to already have broken in the first cycle. FIBRE 2 (grey) breaks after many cycles caused by the stress concentration field of the debond crack tip of FIBRE 1. Adapted from [5].

FIBRE 1 in the first loading cycle. It is assumed that FIBRE 1 fails early in this loading step. After FIBRE 1 has broken, a debond crack will form at the fibre-matrix interface and grow with increasing strain $\bar{\varepsilon}$. During that loading, the debonded fibre exhibits a slip in the positive z-direction (forward slip) resulting in the frictional sliding shear stress τ_s that will act in the opposite direction of the forward slip direction. For the first loading, the shear stress is a material constant and denoted as τ_s^0. Once $\bar{\varepsilon}$ reaches $\bar{\varepsilon}_{max}$, the debond reaches the initial length after the first cycle, denoted as l_d^0. Based on [6], the initial debond length l_d^0 at the maximum strain $\bar{\varepsilon} = \bar{\varepsilon}_{max}$ can be calculated as follows:

$$\frac{l_d^0}{r} = \frac{E_f}{2\tau_s^0}\left(\bar{\varepsilon}_{max} - \frac{\bar{\sigma}_i}{E_c}\right), \tag{1}$$

with r as fibre radius, E_f as fibre Young's modulus, τ_s^0 as interfacial shear stress at first loading, $\bar{\varepsilon}_{max}$ as maximum applied macroscopic strain, $\bar{\sigma}_i$ as debond initiation stress and E_c as the composite Young's modulus given by the rule of mixtures. The debond initiation stress defines the macroscopic stress at which a debond crack growth can initiate. It is introduced based on [4]:

$$\frac{\bar{\sigma}_i}{E_c} = \frac{(1-V_f)E_m}{E_c}\Delta\varepsilon^T + 2\sqrt{\frac{(1-V_f)E_m}{E_c}\left(\frac{G_c^i}{E_f r}\right)}, \tag{2}$$

with E_m as the matrix Young's modulus, $\Delta\varepsilon^T$ as the thermal mismatch strain and G_c^i as the interfacial fracture energy of the debond crack tip. $\Delta\varepsilon^T$ is a measure for the difference in thermal expansion along the fibre direction of fibres and the matrix.

As can be seen from Equation 1 and Equation 2, the initial debond length is mainly influenced by the interfacial properties τ_s^0 and G_c^i and the thermal mismatch strain $\Delta\varepsilon^T$.

Subsequent Loading and Debond Growth After the first load cycle, the two-fibre composite is unloaded to the minimum applied macroscopic strain $\bar{\varepsilon}_{min}$ and subsequently loaded cyclically. $\bar{\varepsilon}_{min}$ can be defined by convention using the R-ratio $R = \bar{\sigma}_{min}/\bar{\sigma}_{max} = \bar{\varepsilon}_{min}/\bar{\varepsilon}_{max}$ for linear elastic materials. For simplicity of this first approach, it is assumed that the critical event of a debond crack tip triggering a fibre break in a neighbouring fibre happens at maximum applied strain under forward slip. The main difference between

1. define the simulation domain
2. discretise the simulation domain (meshing)
3. define the material properties for fibre, matrix and intact interface
4. set the thermal prestress
5. calculate the maximum debond length (saturation length)
6. set the first fibre to be broken
7. initiate the fibre break and debond for all broken fibres
   a) initiate a break in the current fibre
   b) calculate the debond length for the current fibre
   c) calculate the material properties for the debonded region for the current fibre
   d) repeat for all broken fibres
8. run the finite element simulation
9. evaluate the stress state for all fibres
   a) evaluate if the current fibre broke, if yes: set this fibre to be broken
   b) repeat for all fibres
10. calculate the next increment size and increase the number of total cycles
11. repeat until all fibres have broken or all fibre debonds are saturated

Figure 2: Flowchart of the methodology. Steps associated with the numerical model are highlighted in blue. Steps associated with the analytical model are highlighted in grey.

loading for the first time and loading after many cycles arises from an additional sticking effect near the debond crack tip [5]. In the scope of this work, this additional sticking effect will not be explicitly modelled in subsequent loading cycles. Nevertheless, due to the way of how the behaviour of the debonded interface will be implemented in the FE model, a sticking effect can be incorporated in future investigations. With these prerequisites, the analytical model for first loading has to be adapted by the cycle-dependent variables. Referring to [6], the interfacial shear stress τ_s decreases during cyclic loading due to a decreasing surface roughness (wearing effect). During first loading, $\tau_s = \tau_s^0$ holds as described earlier. After many load cycles, the interfacial shear stress reaches a constant value $\tau_s = \tau_s^c$. The transition from τ_s^0 to τ_s^c is described by a simple decay law [6]:

$$\tau_s(\mathcal{N}) = \begin{cases} (\tau_s^0 - \tau_s^c)\left(1 - \left(\frac{\mathcal{N}}{\mathcal{N}_c}\right)^n\right) + \tau_s^c & \text{for } \mathcal{N} < \mathcal{N}_c \\ \tau_s^c & \text{for } \mathcal{N} \geq \mathcal{N}_c \end{cases}, \tag{3}$$

with $\mathcal{N}$ as the number of cycles since the fibre broke, $\mathcal{N}_c$ as the number of cycles to reach τ_s^c and n as a decay exponent. Here, it has to be mentioned that each fibre is assigned its own cycle count after fibre break which consequently is different from the total cycle count N of the entire composite ($\mathcal{N} \neq N$). $\mathcal{N} = 0$ for the cycle in which the fibre broke.

Equation 1 can be extended to calculate the current debond length $l_d(\mathcal{N})$ based on the current shear stress $\tau_s(\mathcal{N})$ [6]:

$$\frac{l_d(\mathcal{N})}{r} = \frac{E_f}{2\tau_s^0}\left(\frac{\bar{\varepsilon}_{max}}{2}\left((1+R) + (1-R)\frac{\tau_s^0}{\tau_s(\mathcal{N})}\right) - \frac{\bar{\sigma}_i}{E_c}\right). \tag{4}$$

Comparing Equation 4 with Equation 1, it becomes obvious that Equation 4 reduces to Equation 1 for $\tau_s(\mathcal{N}) = \tau_s^0$. It follows, that as τ_s decreases, l_d increases until l_d reaches

the saturated debond length l_d^c when $\tau_s = \tau_s^c$. If fibre failure has not occured in FIBRE 2, the fatigue damage is stable.

2.3 Adapted Cohesive Law for Debonded Interface (7c)

It has been shown in subsection 2.2 that the interface region between the fibres and the matrix is crucial for the microscopic failure mechanisms. Therefore, a precise way of numerically modelling the constitutive response of this region is needed while keeping the computational costs low due to the cyclic nature of the problem. Therefore, a traction-separation law for cohesive elements is used to describe the material behaviour in the bonded and debonded interface region. This is numerically less expensive than modelling a discrete contact with friction in the debonded region as has been done in the appendix of [5].

It is assumed that the properties of the bonded region do not change during a single cycle. Accordingly, the bonded region is modelled using a single thin layer of hexahedral cohesive elements without damage. The linear elastic response of the cohesive elements is defined by the stiffness vector $\mathbf{K} = (K_n, K_s, K_t)^\top$ consisting of the normal component K_n and the shear components in two directions K_s and K_t. To simulate a perfect bonding, displacement continuity at the interface is achieved by setting all components of the stiffness vector to a high value $\mathbf{K} = \mathbf{1} \times \mathbf{10^8}$ MPa.

The debonded region exhibits a combination of sticking and slipping friction. Therefore, the cohesive element should behave linear elastically until a maximum shear traction t^0 is reached at the corresponding separation δ_0. If the separation δ further increases by the increment $\Delta\delta_0$, the shear traction t should remain constant. This behaviour is depicted in Figure 3a. The slope of the linear elastic regime (the sticking region) can be modelled by the shear components of $\mathbf{K}$. As the cohesive element should be quasi-indeformable in normal direction, the normal component of K is set to a high value of 1×10^8 MPa. The damage initiation is handled by a quadratic nominal stress criterion as described in [3]. Herein, the traction values for onset of damage t_s^0 and t_t^0 are set according to the interface behaviour, t_n^0 is set to a high value of 1000 MPa. This way, the influence of the normal traction on the quadratic nominal stress criterion can be reduced and thus the shear tractions dominantly determine the interface behaviour.

After the onset of damage, the constant traction behaviour can be modelled by introducing a dependency between the damage variable D and the separation $\Delta\delta$:

$$D = 1 - \frac{\delta^0}{\delta^0 + \Delta\delta}, \text{ with } \delta^0 + \Delta\delta = \delta. \tag{5}$$

An exemplary relation between $\Delta\delta$ and D is depicted in Figure 3b.

Modelling perfect bonding in the bonded interface region and a capping shear traction in the debonded interface region together with the sharp transition from one region to another caused by assigning different materials to neighbouring cohesive elements allows for a quasi-singular (in the scope of an FE simulation) crack tip stress field.

2.4 Hybrid Analytical-Numerical Model (all steps)

The previous sections described the prerequisites for implementing the fatigue mechanism for UD-FRPs in a hybrid analytical-numerical model. This section will again refer

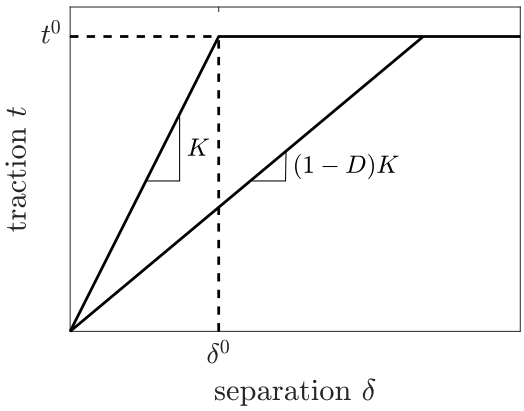

(a) Linear elastic and subsequent constant traction behaviour.

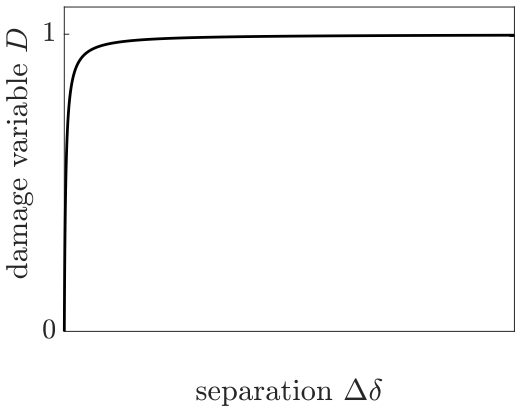

(b) Dependency of the damage variable D on the separation $\Delta\delta$.

Figure 3: Bi-linear traction-separation material model for debonded interface regions.

to Figure 2 but focus on the detailed numerical implementation of the necessary steps to summarise the entire model workflow in detail.

Definition and Discretisation of the Simulation Domain (1, 2) The two-fibre composite from Figure 1 is used as a baseline for the simulation domain to explain the workflow. However, if the two-fibre composite is to be modelled using finite elements while maintaining a relevant fibre volume fraction of $V_f > 0.5$, the distance between the outer diameter of the fibre and the outer boundary of the simulation domain would become small resulting in edge effects. Therefore, a concentric frame of fibre material is added around the matrix material mimicking the stiffening effect of the neighbouring fibres in a real composite. The dimensions of this so-called fibre frame can be adjusted so that the two-fibre model has the desired fibre volume fraction leading to a simplified model with comparable mechanical conditions as in a real composite.

To facilitate the symmetrical problem, only half the problem domain is used as simulation domain. The two-fibre composite domain is meshed using linear, reduced integration, hexahedral elements with enhanced hourglass control (C3D8R). The interface regions between the fibre and the matrix are meshed using hexahedral cohesive elements (COH3D8). The element size along the z-direction is set equal for every element. The simulation domain is depicted in Figure 4.

Definition of the Cycle-Independent Material Properties (3) In this first investigation, the cycle-independent materials (fibre, matrix and bonded interface do not change their material behaviour between cycles) are modelled using linear elastic relations. As a finite element framework is used, the material models can later easily be exchanged by more advanced constitutive relations. To allow for fibre breakage, a failure criterion for the fibres has to be determined additionally. Therefore, the fibre elements are assigned a strength in fibre direction σ_{ult}. As will be shown later, the fibre breakage is judged by postprocessing the results of a linear elastic simulation. Consequently, the strength

properties are defined outside of the FE model. As fibres fail from local defects, the material properties of the fibres have to locally vary following a statistical distribution. Only that way, a K-field can trigger a break in a neighbouring fibre. Assuming the fibres fail from a surface defect [6] and that it is insignificant, where that defect is located at the circumference of the fibre, all elements of a cross section of the fibre are assigned the same material properties. This leads to "discs" of same Young's modulus and same strength as shown in Figure 4b. The Young's modulus of the fibres is assumed to follow a normal distribution and the strength is assumed to follow a two-parameter Weibull distribution. Whereas the normal distribution does not show a length-scale dependency, the Weibull distribution does. Therefore, if the strength distribution is determined experimentally on specimens with a reference length L_{ref}, a strength drawn from this distribution has to be scaled to the size of the single material element disc of the FE simulation. In this work, the characteristic strength of each element is scaled according to the element length along the z-direction using the following relation [9]:

$$\sigma_{ult}(L) = \sigma_{ult}(L_{ref}) \left(\frac{L_{ref}}{L} \right)^{\frac{1}{m}}, \tag{6}$$

with L as the scaled length, L_{ref} as the reference length, $\sigma_{ult}(L)$ as the scaled strength of the element, $\sigma_{ult}(L_{ref})$ as the reference strength and m as the Weibull modulus.

For each disc, a Young's modulus is drawn as a sample from the normal distribution and a strength is drawn as a sample from the Weibull distribution and scaled according to Equation 6. The number of material discs is determined by the number of elements along the z-direction in the simulation domain (in Figure 4b: 137). The fibre frame is not subjected to statistically varying material parameters as fibre fracture is prevented in this region. Accordingly, the fibre frame is assigned a mean linear-elastic fibre material with no failure strength. The following material parameters have to be defined: the mean and the standard deviation of the Young's modulus distribution of the fibres $\sigma(E_f)$ and $\mu(E_f)$, the Weibull scale and shape parameter of the strength distribution of the fibres $A(E_f)$ and $B(E_f)$, the Poisson's ratio of the fibres ν_f, the Young's modulus of the matrix E_m and the Poisson's ratio of the matrix ν_m.

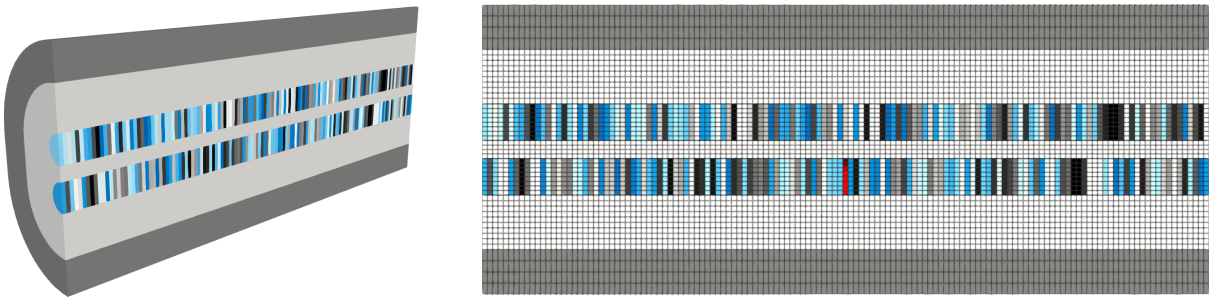

(a) Overview. The mesh is hidden for better visibility.

(b) Side view with the initial fibre break in the centre and the debonded region in red.

Figure 4: Exemplary discretised two-fibre composite with fibre frame. The blue colours represent the statistical distribution of the fibre properties.

Initiation of the Thermal Prestress (4) As the matrix and the fibres have different coefficients of thermal expansion, residual stresses form during cool-down from processing temperature. The way of determining this residual stress shall not be described herein. Following subsection 2.2, the definition using the mismatch strain is used. For further information, the reader is referred to [4].

Calculation of the saturated debond length (5) As the two-fibre composite consists of two equal fibres with equal interface properties, both fibres will have the same saturated debond length l_d^c. Thus, it has to be calculated only once at the beginning of the workflow using Equation 4 and Equation 3 with $\mathcal{N} = \mathcal{N}_c$.

Setup of the First Loading Cycle (6, 7) To start the fatigue process, FIBRE 1 in the two-fibre composite is initiated with a fibre break in the centre of the simulation domain $z_{break,1} = l_{model}/2$. This is implemented by deleting the material disc closest to $z_{break,1}$ as shown in Figure 4a. Subsequently, the initial debond length of FIBRE 1 is calculated using Equation 1 and Equation 2. The material properties of the cycle-dependent debonded interface region are initialised by setting the maximum shear tractions equal to the initial interfacial shear stress $t_s^0 = t_t^0 = \tau_s^0$. The maximum normal traction is set to $t_n^0 =$ 1000 MPa, the normal stiffness is set to $K_n = 1 \times 10^8$ MPa as described in subsection 2.3. For future investigations, the sticking behaviour can be adjusted by adapting K_s and K_t to the analytical behaviour. In the scope of this work, $K_s = K_t = 1 \times 10^6$ MPa is used. The interface elements are assigned either the bonded or the debonded interface material properties based on their z-position. If the element centre lies within a distance of $l_d^0/2$ of the fibre break, the elements are assigned the debonded material properties. Else, they are assigned the bonded material properties.

Setup of Subsequent Loading Cycles (6, 7) In subsequent cycle steps, the debond of any of the two fibres has grown due to the cycles in previous steps. Thus, the current debond length and the current interfacial shear stress are recalculated using Equation 4 and Equation 3 respectively for the current cycle count $\mathcal{N}$ for each fibre. Subsequently, the material properties for the bonded and debonded interface region are recalculated and reassigned based on the the current interfacial shear stress $\tau_s(\mathcal{N})$ and the current debond length $l_d(\mathcal{N})$.

The procedure of initiating a fibre break after the first loading cycle is comparable to the first fibre break in the first cycle. If a fibre was determined to have broken in the previous cycle step (i.e. the stress in fibre direction in the last cycle step exceeded the strength of the respective element), the failed fibre disc is deleted from the simulation. The initial debond length is calculated and the bonded and debonded interface properties are assigned based on τ_s^0.

Simulation and Evaluation of the Current Cycle (8, 9, 10) The previous steps are needed to set up the actual FE simulation for the current cycle. This simulation consists of two static, implicit simulation steps: first an equilibrium step to achieve equilibrium after the thermal mismatch in fibres and matrix and secondly a displacement step to apply

the maximum macroscopic strain $\bar{\varepsilon}_{max}$. The displacement is applied on the z-component of the nodes at the positive end of the domain: $U^z_{z+} = l_{model}\ \bar{\varepsilon}_{max}$. Further boundary conditions prevent a translational movement of the simulation domain by setting the z-displacement of the nodes at the negative end of the domain to 0: $U^z_{z-} = 0$. The nodes in the centre of the simulation domain ($x = y = 0$) are constrained to only allow an elongation along the z-direction: $U^x_{x=y=0} = U^y_{x=y=0} = 0$. Poisson effects are not restricted. An x-symmetry boundary condition is applied to the symmetry plane.

One simulation is created per cycle step. There is no transfer of information between the cycle step simulations except the difference in fibre breaks, debond lengths and debonded interface properties. This is justifiable without restriction for linear elastic material properties but has to be kept in mind and thoroughly investigated when implementing history-dependent material properties like plasticity.

After the simulation was carried out, each element of each fibre is evaluated for failure. Therefore, the element stress in z-direction σ_{zz} is compared to the respective element strength σ_{ult}. If $\sigma_{zz} > \sigma_{ult}$, the entire fibre disc is labelled as "broken" to be removed in the next cycle step. Additionally, the current total cycle count N is stored as debond initiation for the respective fibre.

Finally, the increment size for the next cycle step is calculated. As the simulation domain is discretised, the debonds can only grow in certain increments. The smallest possible debond crack growth Δl_d per cycle step equals the element length in z-direction. With Equation 4, the number of cycles necessary to make a debond grow this minimal increment size (one element length) can be determined solving the inverse problem $\mathcal{N}(l_d)$.

Subsequently, the current cycle is increased by the cycle increment and the next simulation can be set up. This procedure is repeated until both fibres in the simulation domain broke or all debonds reached the saturated debond length indicating fatigue run-out.

3 Model Results

3.1 Development of the Neighbouring Fibre Stress

With the proposed workflow, the microscopic mechanisms of fatigue damage can be investigated in detail. The material parameters used herein and their source are denoted in Table 1. A first investigation focuses on the development of the fibre stress in a neighbouring fibre (denoted as Fibre 2) of an already broken fibre (denoted as Fibre 1). As was shown by [8], the stress in the neighbouring fibre shows three distinct stress peaks. One at the fibre break location of Fibre 1 and one each near the debond crack tip location of Fibre 1. Only if the proposed model can depict this behaviour, the mechanism of a fibre debond crack tip triggering a neighbouring fibre break can also be depicted. Therefore, a simulation domain with $l_{model} = 40\ r$, $d_{if} = r$ and $r = 0.017$ mm is generated as shown in Figure 4a. Load is applied with a maximum macroscopic strain $\bar{\varepsilon}_{max} = 0.02$ and $R = 0.1$. As it is not necessary to trigger a fibre break in this investigation, the statistical material properties are neglected. Consequently, all fibre elements are assigned the same linear elastic material properties. Simulations are carried out for $N = 1, 10000, 20000, 30000$ and 40000. As the maximum stress in Fibre 2 occurs at the elements closest to Fibre 1, the stresses in z-direction in those elements are investigated. Additionally, they are normalised to the far field stress determined at the boundaries ($z+$

and $z-$) of the simulation domain. It has to be noted that, depending on the domain size, the stress at the boundaries can differ from the actual far field stress. This influence is assumed to be negligible for the used discretisation. The results are depicted in Figure 5a.

Table 1: Material parameters used for the E-glass fibres, the matrix and the interface region. * only used in statistical simulation. [a] measured values for EPIKOTE™ Resin MGS™ RIMR 135 + EPIKURE™ Curing Agent MGS™ RIMH 137 from Hexion Inc., Columbus, OH, USA; [b] measured values for Hybon™ 2150 from Nippon Electric Glass Co., Ltd., Ōtsu, Japan; [c] assumed values in order of magnitude of [6]; [d] value from [10].

E_m [MPa]	ν_m [−]	$\mu(E_f)$ [MPa]	$\sigma(E_f)$* [MPa]	$A(\sigma_{ult,f})$* [MPa]	$B(\sigma_{ult,f})$* [MPa]	ν_f [−]
3019[a]	0.39[a]	72381[b]	797[b]	2103[b]	6[b]	0.2[d]
V_f [−]	$\Delta\varepsilon^T$ [−]	G_c^i [J/m^2]	τ_s^0 [MPa]	τ_s^c [MPa]	N_c [−]	n [−]
0.6[c]	0.0033[c]	50[c]	75[c]	5[c]	50000[c]	0.9[c]

As can be seen, the model develops three stress peaks in Fibre 2. This is in qualitative agreement with findings from the literature [8]. It can further be noted, that the secondary stress peaks form during cyclic loading. Whereas for $N = 1$, only one stress peak at the location of the break in Fibre 1 is present, this shifts towards three distinct stress peaks for $N = 40000$. Investigating the position of the secondary stress peaks relative to the debond crack tip in Fibre 1, the model shows the stress peak shifted towards the position of the break in Fibre 1. This can be explained by the redistribution of the stress in the model composite after Fibre 1 broke. As the fibres have an inter-fibre spacing, the matrix is transferring a part of the load from broken Fibre 1 to intact Fibre 2. A superposition of the macroscopic load and the K-field of the debond crack tip in Fibre 1 lead to the shifted peak stress positions.

3.2 Initiation of a Neighbouring Fibre Break

As the model can predict the characteristic three stress peaks in the neighbouring fibre, a second investigation is carried out using statistical fibre properties and allowing a fibre break in Fibre 2. To increase the probability of a fibre break within the simulation domain, the reference length for Weibull scaling is set to $L_{ref} = l_{model}$. The simulation domain remains the same as in the first investigation.

As can be seen in Figure 6, the model can initiate a fibre break in Fibre 2 having been triggered by the debond crack tip of Fibre 1. Fibre 2 breaks at cycle $N = 40410$. A stress exposure is defined as the ratio between the element stress in fibre direction and the element strength σ_{zz}/σ_{ult}. The stress exposure for the critical element (the to-break element in Fibre 2) and the element at the z-position of the break in Fibre 1 (centre element) is depicted in Figure 5b. It can be seen that the stress exposure of the critical element remains approximately the same until $N \approx 30000$. After that, the K-field of

the debond crack tip moves into the proximity of the critical element. As soon as the exposure in the critical element exceeds 1, the element fails creating a break in Fibre 2. The stress exposure in the centre element gradually decreases until the break of Fibre 2. Subsequently, the stress exposure drops. This is according to expectation.

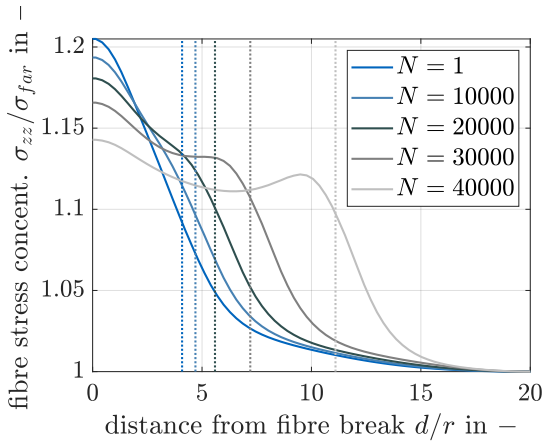

(a) Fibre stress along Fibre 2 for equal material properties in the fibres. Only half the simulation domain is plotted.

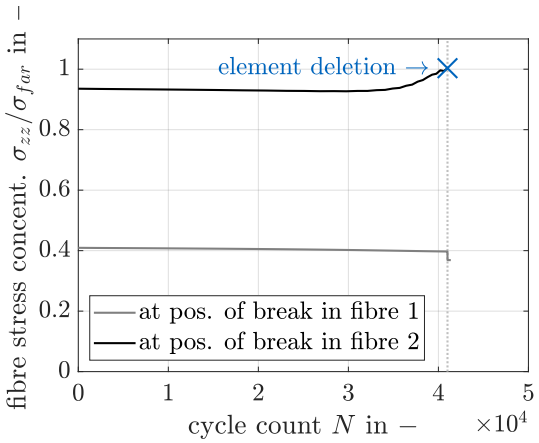

(b) Stress exposure in Fibre 2 for statistical material properties.

Figure 5: Model results.

(a) At $N = 1$ (after Fibre 1 broke).

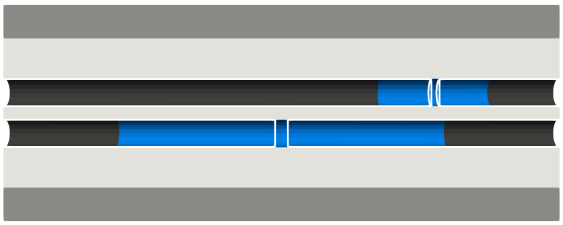

(b) At $N = 40411$ (after Fibre 2 broke).

Figure 6: Debond crack growth results. The fibres are shown by a white outline. Debonded interface regions are blue. Bonded interface regions are black.

4 Conclusion

A model for investigating the micromechanical fatigue behaviour of unidirectional composites based on fibre-matrix debonding was proposed. The model uses an analytical approach do determine the debond crack initiation and growth and a numerical finite element approach to calculate resulting stresses. The model can qualitatively predict the development of stresses in a neighbouring fibre of a broken fibre. Additionally, the model can depict the process of a debond crack tip stress field triggering a break in a neighbouring fibre. Latter is consistent with the microscale observations in the literature [7]. A quantitative validation of the model with experimental data is still to be carried

out. Future work could investigate the model behaviour under history-dependent material models for the matrix and statistically distributed multi-fibre simulation domains.

5 Acknowledgements

The authors thankfully acknowledge the funding provided by the German Federal Ministry of Education and Research in the framework of the project SensoTwin (funding code: 13XP5121A).

REFERENCES

[1] P. Brøndsted, H. Lilholt, and A. Lystrup. COMPOSITE MATERIALS FOR WIND POWER TURBINE BLADES. *Annual Review of Materials Research*, 35(1):505–538, 2005.

[2] S. Korkiakoski, P. Brøndsted, E. Sarlin, and O. Saarela. Influence of specimen type and reinforcement on measured tension–tension fatigue life of unidirectional GFRP laminates. *International Journal of Fatigue*, 85:114–129, 2016.

[3] Dassault Systèmes Simulia Corp. Abaqus Documentation Version 2020: Abaqus Analysis User's Guide. 2020.

[4] B.F. Sørensen. Micromechanical model of the single fiber fragmentation test. *Mechanics of Materials*, 104:38–48, 2017.

[5] B.F. Sørensen and S. Goutianos. Micromechanical model for prediction of the fatigue limit for unidirectional fibre composites. *Mechanics of Materials*, 131:169–187, 2019.

[6] B.F. Sørensen, S. Goutianos, L.P. Mikkelsen, and S. Fæster. Fatigue damage growth and fatigue life of unidirectional composites. *Composites Science and Technology*, 211:108656, 2021.

[7] K.M. Jespersen and L.P. Mikkelsen. Three dimensional fatigue damage evolution in non-crimp glass fibre fabric based composites used for wind turbine blades. *Composites Science and Technology*, 153:261–272, 2017.

[8] P.W.J. van den Heuvel, T. Peijs, and R.J. Young. Failure phenomena in two-dimensional multi-fibre microcomposites–3. A raman spectroscopy study of the influence of interfacial debonding on stress concentrations. *Composites Science and Technology*, 58(6):933–944, 1998.

[9] S. Feih, K. Wonsyld, D. Minzari, P. Westermann, and H. Lilholt. Testing procedure for the single fiber fragmentation test. Risø National Laboratory. Denmark. Risø-R-1483(EN).

[10] A.S. Kaddour and M.J. Hinton. Input data for test cases used in benchmarking triaxial failure theories of composites. *Journal of Composite Materials*, 46(19-20):2295–2312, 2012.